JEECS (Journal of Electrical Engineering and Computer Sciences)
Vol. 11, No. 2, December 2026, pp. 196-207
e-ISSN: 2579-5392 p-ISSN: 2528-0260

Design, Implementation, and Simulation-Based Performance Evaluation of an Automatic Dual-Axis Solar Tracking System for Small-Scale Photovoltaic Applications

Bui Hoang Man[1,2], Tran Van Duc[1], Nguyen Huu Bao Thinh[1], Phan Ton Thanh Tam[1], Nguyen Thi Kim Anh[1], Ho Van Dung[1,3]

[1]Faculty of Engineering and Food Technology, Hue University of Agriculture and Forestry, 102 Phùng Hưng, Phú Xuân, Huế, Vietnam

[2]Scavi Hue Company, Phong Dien Industrial Park, Phong Dien Ward, Hue City, Vietnam

[3]Department of Agricultural Engineering, Faculty of Engineering at Kamphaeng Saen, Kasetsart University, Tambon Kamphaeng Saen, Kamphaeng Saen District, Nakhon Pathom, Thailand

Article Info

Article history:
Received: 8 August 2026
Revised: 7 November 2026
Accepted: 13 November 2026

Keyword:
Arduino UNO
Dual-Axis Solar Tracker
Light-Dependent Resistor
Photovoltaic System
Simulink

Abstract

Fixed-tilt photovoltaic (PV) panels cannot follow the daily motion of the sun, which increases the angle of incidence and causes cosine losses, especially in the early morning and late afternoon. Dual-axis solar trackers can reduce this loss; however, many reported systems are either too complex and costly for small-scale users, or are evaluated only through hardware demonstrations or simulations under ideal assumptions, without a clear link between the prototype and the expected energy gain. This study presents the design, implementation, and simulation-based performance evaluation of a low-cost automatic dual-axis solar tracking system for small-scale PV applications. Its main contribution is a combined framework that links a functionally validated Arduino-based prototype, using a four-quadrant LDR array and two-axis electromechanical actuators, with a MATLAB/Simulink comparison of fixed and ideal dual-axis configurations under identical input conditions. Laboratory tests with an artificial light source confirmed correct actuator responses in all five test conditions. Over a simulated 12-hour daytime period, the accumulated energy increased from 142.80 Wh to 181.82 Wh, a 27.32% improvement. Because the simulation assumes ideal tracking and does not include actuator energy consumption, this value is an upper-bound estimate, and outdoor measurements are needed for confirmation.

Corresponding author:
Ho Van Dung, hovan.d@ku.th; hovandung@huaf.edu.vn

DOI: https://doi.org/10.54732/jeecs.v11i2.9

This is an open access article under the CC–BY license.

1. Introduction

Solar energy has become an important renewable energy source for residential, agricultural, and industrial applications due to its widespread availability and environmental benefits [1], [2]. However, most PV panels are installed in fixed positions. Because the sun's position changes continuously during the day and across seasons, a fixed panel cannot maintain an optimal orientation, which increases the angle of incidence and limits energy harvesting [3]. Automatic solar tracking systems have therefore been developed to keep the panel facing the sun, and dual-axis trackers offer the highest theoretical gain at the cost of higher complexity, cost, and power consumption [4]–[8].

Previous research on PV solar tracking can be grouped into three directions. First, review studies have summarized tracker types, drive mechanisms, and control strategies, and generally report that dual-axis trackers provide the highest energy gain at the cost of additional complexity and power consumption [4]–[8]. Second, low-cost Arduino- and LDR-based prototypes have shown that sun tracking can be achieved

with simple sensing and actuation, and some of them add IoT monitoring or a fixed-versus-tracking comparison [2], [7], [9]. Third, simulation-oriented studies have modeled PV modules in MATLAB/Simulink to analyze the output power under varying irradiance [1, 3, 9]. Recent studies published in 2026 continue along these directions. Lin et al. [10] designed a dual-axis tracking mechanism for a 1 kW unit using SolidWorks and finite element analysis, and reported a maximum stress of 27 MPa, well below the 245 MPa yield strength, under typhoon and earthquake loads. Athara et al. [11] developed an Arduino–LDR dual-axis tracker with INA219 voltage and current monitoring and compared it with a static panel. Taha et al. [12] proposed an energy-aware PID tuning framework that includes actuator energy in the control objective. Chenchireddy et al. [13] developed an Arduino- and LDR-based dual-axis tracker with four light sensors and servo motors. Recent reviews also note that LDR-based trackers are low-cost and require little processing, but are less robust than vision-based approaches under variable lighting [14].

However, these studies still have clear limitations. Review papers [4]–[8] summarize the technology but do not provide a reproducible low-cost design for small-scale users. Low-cost prototypes [2], [9] are mostly evaluated by checking whether the actuators move toward the light source, and the expected energy gain is not quantified. Simulation studies [1], [3], [15] usually focus on PV modeling or assume ideal tracking without a link to an implemented prototype. Among the 2026 studies, Lin et al. [10] concentrate on structural strength and do not evaluate the electrical performance; Taha et al. [12] focus on controller tuning evaluated by simulation rather than on a low-cost hardware build; and Athara et al. [11] combine a prototype with simulation, but state that tests under real weather conditions and the energy consumption of the tracking system remain to be examined.

Therefore, the research gap addressed in this study is the lack of a small-scale dual-axis tracker that (i) is built from low-cost and commonly available components, (ii) is functionally verified at the prototype level with a clearly defined control logic, and (iii) is connected to a transparent MATLAB/Simulink comparison with a fixed panel under identical input conditions. This is important for small-scale users such as households and small farms, who cannot afford complex controllers or expensive commercial trackers, but still need an estimate of the expected energy gain before investing in a tracking system.

This study aims to design and implement a low-cost automatic dual-axis solar tracking system for small-scale PV applications and to evaluate its potential performance improvement through MATLAB/Simulink simulation. The proposed system integrates an Arduino UNO R3, a four-quadrant LDR sensor array, a JGY370 DC gear motor, an MG996R servo motor, an L298N motor driver, and an LM2596 buck converter [13]. The main contributions are: (1) a low-cost dual-axis tracker design with a defined control algorithm; (2) a functional validation of the prototype under five light-source conditions; (3) a MATLAB/Simulink model that compares fixed and dual-axis PV configurations under identical conditions; and (4) a quantified upper-bound estimate of the energy gain, together with a discussion of the remaining limitations. The rest of the paper is organized as follows: Section 2 describes the methodology, Section 3 presents and discusses the results, and Section 4 concludes the paper.

2. Research Methodology

2.1. Overall System Operational Principle

The operational framework of the proposed dual-axis solar tracking system is fundamentally based on the photovoltaic effect, converting solar irradiance into electrical energy. When incident solar radiation strikes the polycrystalline photovoltaic (PV) module, direct current (DC) electricity is generated. This generated electrical power is subsequently regulated by a charge controller to safely charge the 12 V battery storage unit, while simultaneously supplying power directly to the connected electrical load. Under low irradiance conditions or during nighttime periods when the generated PV voltage drops below the functional threshold, the system automatically switches to the backup battery storage to ensure an uninterrupted power supply to the load.

Figure 1 separates the energy conversion chain from the feedback control chain. Solar radiation enters the PV module; the charge controller manages battery charging, and the battery–inverter path supplies the AC load. Separately, directional light-sensor signals are processed by the microcontroller, which commands the azimuth and elevation actuators to reposition the PV module.

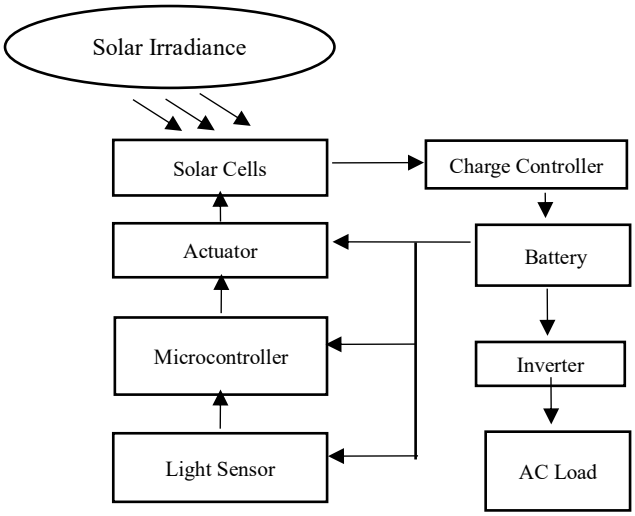

Figure 1. Block diagram of the dual-axis solar tracking system.

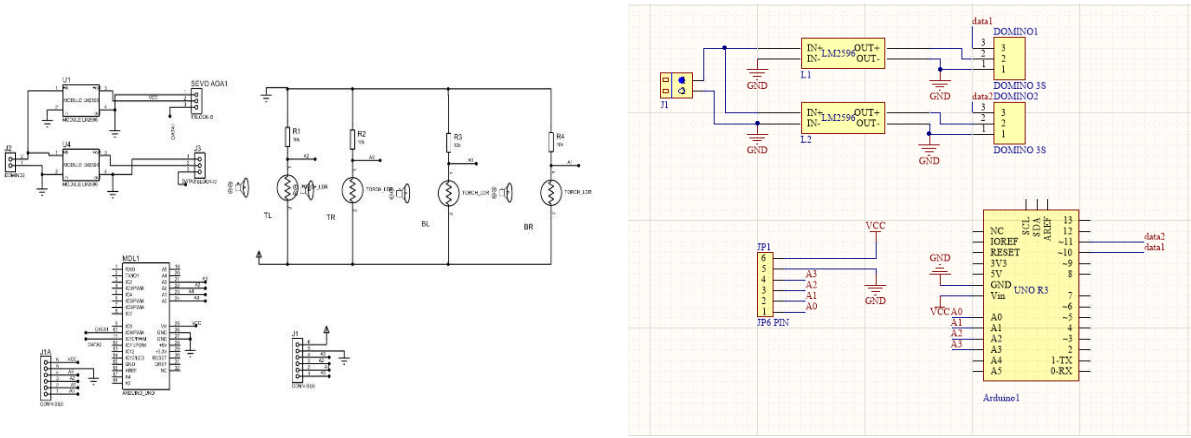

Figure 2. Schematic diagram of the embedded control circuit.

Due to the continuous apparent motion of the sun throughout the day, the solar inclination and azimuth angles vary dynamically, causing significant cosine losses in fixed-tilt configurations. To mitigate this limitation, an automatic embedded control loop is integrated to continuously adjust the solar panel's orientation, minimizing the angle of incidence between the incoming solar rays and the module's surface normal vector. By continuously minimizing the incidence angle between the incoming solar rays and the PV-module surface normal, the tracker maintains an approximately normal orientation toward solar radiation. Under ideal tracking conditions, the incidence angle approaches 0°. The effective solar irradiance captured by the PV module is maximized, thereby significantly enhancing the overall energy harvesting efficiency of the system.

2.2. Embedded Control Circuit Architecture

Figure 2 illustrates the electronic control architecture of the proposed dual-axis solar tracking system, which was developed using low-cost and commercially available components. An Arduino UNO R3, based on the ATmega328P microcontroller, serves as the central controller and processes analog signals from four light-dependent resistors (LDRs). The sensors are arranged in four quadrants and separated by a cross-shaped divider to detect differences in incident light intensity. Each LDR is connected to an analog input through a voltage-divider circuit. The controller compares the left–right and upper–lower sensor readings to determine the directional tracking errors. Based on these errors, the Arduino controls the JGY370 DC geared motor through an L298N H-bridge driver for azimuth adjustment and commands the MG996R servo motor for elevation adjustment. An LM2596 DC–DC voltage regulator provides a regulated supply for the designated low-voltage components. This configuration enables automatic two-axis positioning of the PV module in response to variations in incident solar radiation.

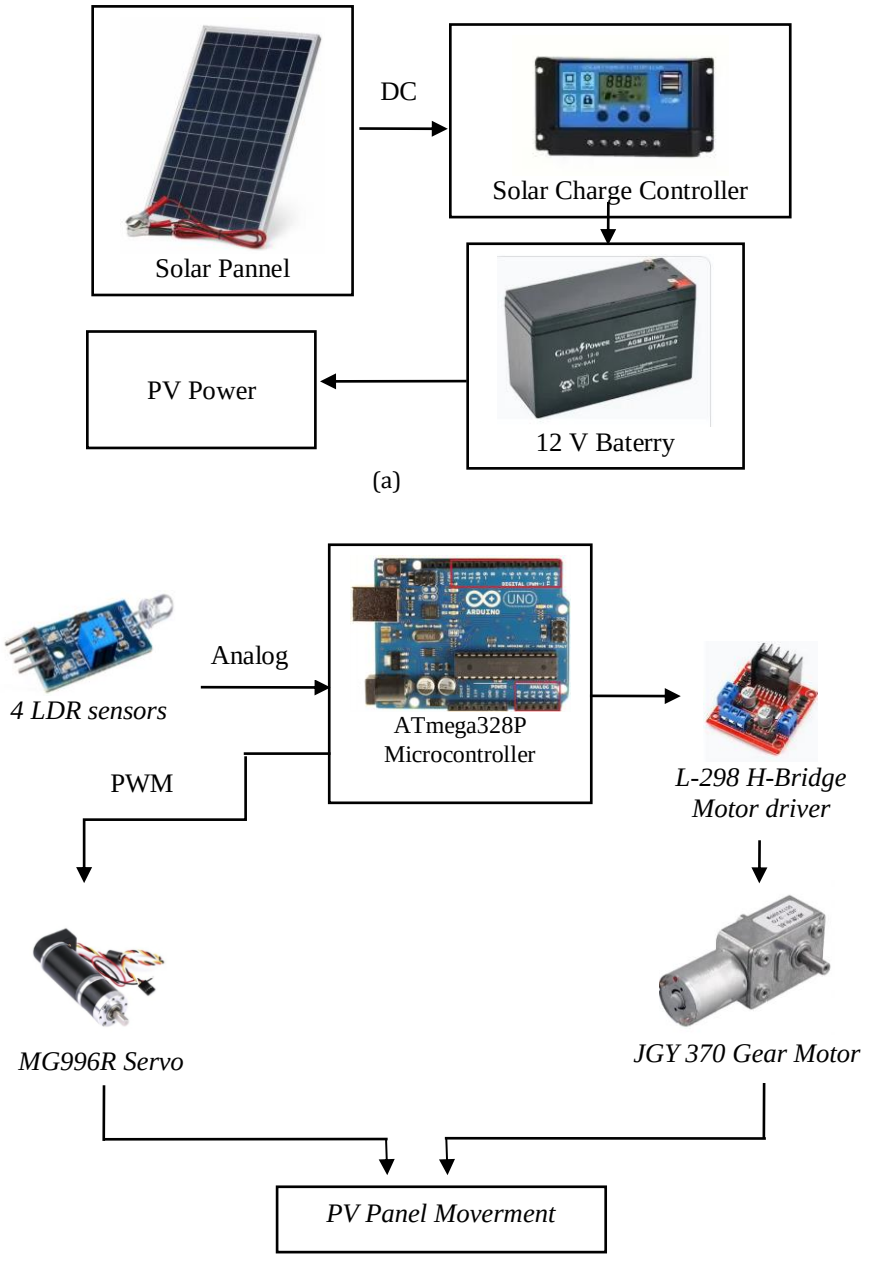

Figure 3. Hardware architecture and principal components of the proposed solar tracking system: (a) PV Power Subsystem; (b) Tracking control system

2.3. Hardware Design and Control Algorithm

The tracking and power management system, as shown in Figure 3, is integrated around the central ATmega328P microcontroller (Arduino UNO). The tracking mechanism utilizes a JGY370 worm gear motor driven through an L298N motor driver module to adjust the panel's position based on light intensity signals received from the 5mm LDR sensor modules. The power supply and distribution unit consists of an LM2596 buck converter to regulate voltage for the control circuitry, a solar charge controller to manage energy storage, and an inverter for power conversion. A PV panel measures and collects solar irradiance for the overall proposed system.

The main hardware components are summarized as follows:

- Controller: ATmega328P Microcontroller (Arduino UNO)
- Light sensors: 5mm LDR Sensor Module
- Actuator: JGY370 Worm Gear Motor
- Motor driver: L298N Motor Driver Module
- Voltage regulator: LM2596 Buck Converter

- Power management: Solar Charge Controller
- Power converter: Inverter
- PV module: PV Panel Solar Irradiance

Main program flowchart

The operational logic and control algorithm of the dual-axis solar tracking system are illustrated in Figure 4. The process continuously monitors light intensity via four LDR sensors and adjusts the horizontal and vertical positions accordingly whenever the calculated error exceeds the predefined tolerance [2], [9].

As shown in Figure 4, the controller first initializes the input/output pins and sets the servo to its starting angle. In each loop it reads the four LDR values and averages them into left, right, upper and lower values. The horizontal error is the difference between the left and right averages, and the vertical error is the difference between the upper and lower averages. Each error is compared with a predefined tolerance. If an error is larger than the tolerance, the JGY370 motor is rotated through the L298N for the horizontal error and the MG996R angle is adjusted for the vertical error; otherwise the actuator stays idle, which avoids unnecessary oscillation around the aligned position. The commanded elevation angle and the azimuth rotation are limited to the mechanical range of the prototype before the loop returns to the sensor reading step.

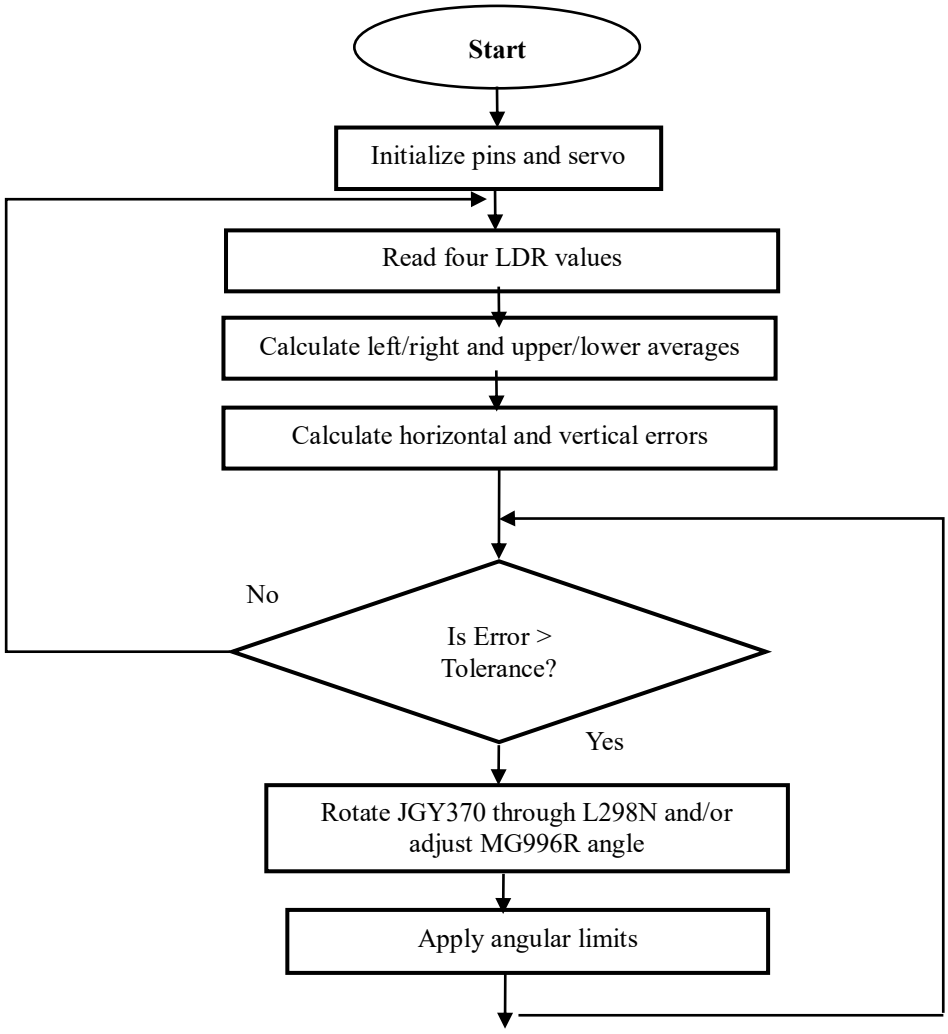

Figure 4. Main program flowchart of the embedded solar tracking controller.

2.4. Mathematical Formulation of the Fixed and Tracking PV Models

To compare the fixed and ideal dual-axis PV configurations under identical inputs, a simplified mathematical simulation was implemented in MATLAB/Simulink. The model uses an assumed daytime irradiance profile, an incidence-angle factor, and the nominal PV-module rating; it does not reproduce a detailed PV equivalent circuit or measure a physical system. The fixed-panel and ideal-tracking calculations are based on solar-incidence relationships discussed in [1], [3], and [15].

For the fixed PV configuration, the effective solar irradiance (G_{eff}) striking the surface of the tilted panel is calculated based on the solar geometry relative to the panel position. The angle of incidence (θ) is mathematically defined as:

$$\cos\theta_i = \sin\alpha_s \cos\beta_p + \cos\alpha_s \sin\beta_p \cos(\gamma_s - \gamma_p) \quad (1)$$

where α_s represents the solar altitude angle, γ_s denotes the solar azimuth angle, β_p is the fixed tilt angle of the PV panel, and γ_p is the panel's fixed azimuth orientation. Consequently, the effective direct normal irradiance component received by the fixed structure is expressed as:

$$G_{fixed} = G_{DNI} \cdot \max(\cos\theta_i, 0) \quad (2)$$

In contrast, the automated dual-axis solar tracking system continuously adjusts its horizontal and vertical orientation to eliminate misalignment. Assuming an ideal tracking mechanism where the orientation error (ϵ) approaches zero ($\theta_{tracking} = 0$), the tracking system continuously positions the PV module perpendicular to the incoming solar rays. Therefore, the effective irradiance available for energy conversion is maximized, yields:

$$G_{tracking} = G_{DNI} \quad (3)$$

For subsequent control sensitivity and precision analysis, any minor orientation deviation caused by the physical embedded control loop can be integrated via:

$$G_{tracking\ actual} = G_{DNI} \cdot \cos(\epsilon) \quad (4)$$

The output electrical characteristics are computed based on the generalized PV power expression. Under standard test conditions (STC), the initial nominal behavior is calculated through:

$$P_{PV} = P_{STC} \cdot \frac{G_{eff}}{1000} \quad (5)$$

where: $P_{STC} = 28\ W$ corresponding to the maximum rating of the polycrystalline module specified in the hardware design, G_{eff} is substituted by G_{fixed} or $G_{tracking}$ accordingly.

For the illustrative half-sine case with a 12 h time window and a peak power of 23.8 W, integration gives E_fixed = P_peak×T/2 = 142.800 Wh and E_dual = P_peak×2T/π ≈ 181.819 Wh. Therefore, (E_dual/E_fixed − 1)×100 = (4/π − 1)×100 ≈ 27.324%. The accumulated energy harvesting over the simulation time horizon (t) is computed by integrating the continuous electrical power output:

$$E_{Wh} = \frac{1}{3600} \int_0^{T_{sim}} P(t)\, dt \quad (6)$$

Finally, the relative energy harvesting improvement indicator (%) is established to quantify the efficiency gain obtained by upgrading from a conventional fixed setup to the proposed dual-axis tracker:

$$\text{Improvement } (\%) = \frac{E_{tracking} - E_{fixed}}{E_{fixed}} \times 100 \quad (7)$$

3. Results and Discussions

3.1. 3D Mechanical Design and Prototype Implementation

To ensure tracking accuracy, a customized light-dependent resistor (LDR) sensor array was engineered to sense real-time micro-variations in daylight intensity. The four quadrant sensors are physically segregated by an orthogonal, cross-shaped shadow divider, which casts distinct shadows when the photovoltaic array is misaligned with the continuous direct solar vector. This spatial arrangement generates differentiated analog voltage inputs to the main embedded microcontroller, which subsequently triggers the azimuth and elevation actuators to mitigate the targeting error. The structural configuration of this sensory element was first modeled in a three-dimensional printed circuit board (PCB) environment to verify electrical routing clearances before undergoing actual physical fabrication. The simulated 3D electronic layout alongside the final physical hardware prototype implementation is successfully displayed in Figure 5.

Following established computer-aided design and prototype fabrication approaches previously applied in small-scale electromechanical system development [16]–[18], the mechanical structure of the proposed solar tracker was modeled using SolidWorks 2018. The CAD modeling focused on developing a rigid supporting frame for the 28 W PV panel and providing the required rotational motion along the azimuth and elevation axes. Mechanical constraints were evaluated to prevent rotational binding along the primary azimuth axis driven by the JGY370 DC gear motor and the elevation axis controlled by the MG996R servo motor. After optimizing the physical component boundaries and tolerances in the simulated environment, the individual mounting brackets and sensor enclosures were manufactured to construct the actual physical prototype framework. The complete isometric engineering illustration showing the numbered component list along with the fully assembled structural hardware prototype is shown in Figure 6.

3.2. Functional Validation of the Prototype

The functional validation was carried out on one prototype in the automatic control engineering practice laboratory of Hue University of Agriculture and Forestry. A light bulb was used as an artificial light source and placed approximately 40 cm from the four-quadrant LDR array. Each of the five conditions in Table 1 was applied three times, and each test lasted 15 minutes. The tests only verify the direction and logic of the actuator responses. Outdoor measurements of the power generated by the prototype were not performed in this study.

The simulation uses an idealized 12-hour daytime profile, with the simulation time t running from 0 h (sunrise) to 12 h (sunset). The irradiance is modeled as a half-sine, $G(t) = G_{peak} \cdot \sin(\pi t/12)$, scaled so that the 28 W polycrystalline module delivers a peak power of 23.8 W at solar noon (t = 6 h), which corresponds to 85% of its rated power. For the fixed panel, the cosine of the incidence angle is taken as $\cos\theta(t) = \sin(\pi t/12)$, so the panel is normal to the sun at noon and the incidence angle increases to 90° at both ends of the day, whereas the ideal tracker keeps $\theta = 0°$. Both configurations use the same irradiance profile and the same module. The results therefore describe an idealized simulated case and not measured field performance, and they do not refer to a specific site, date, panel tilt or azimuth.

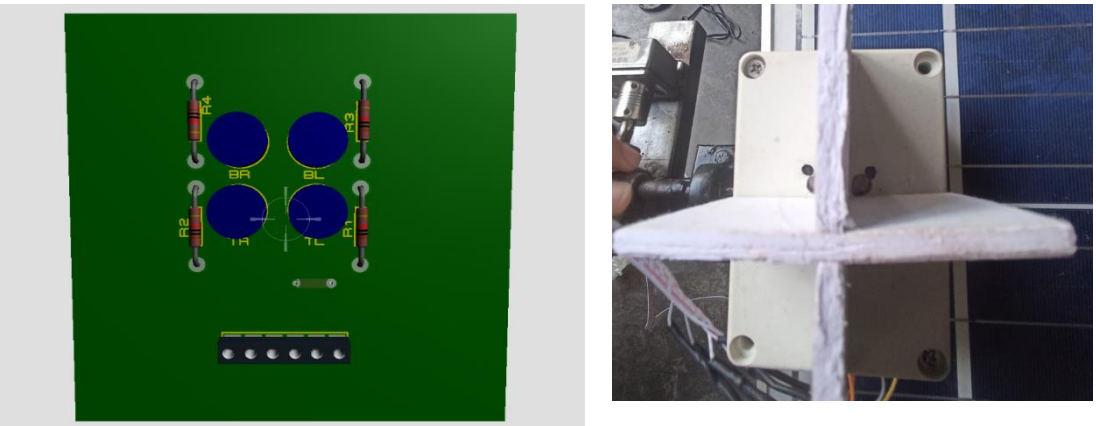

(a) (b)

Figure 5. LDR sensor-array design and physical implementation: (a) 3D PCB visualization and (b) fabricated four-quadrant LDR assembly with a cross-shaped divider.

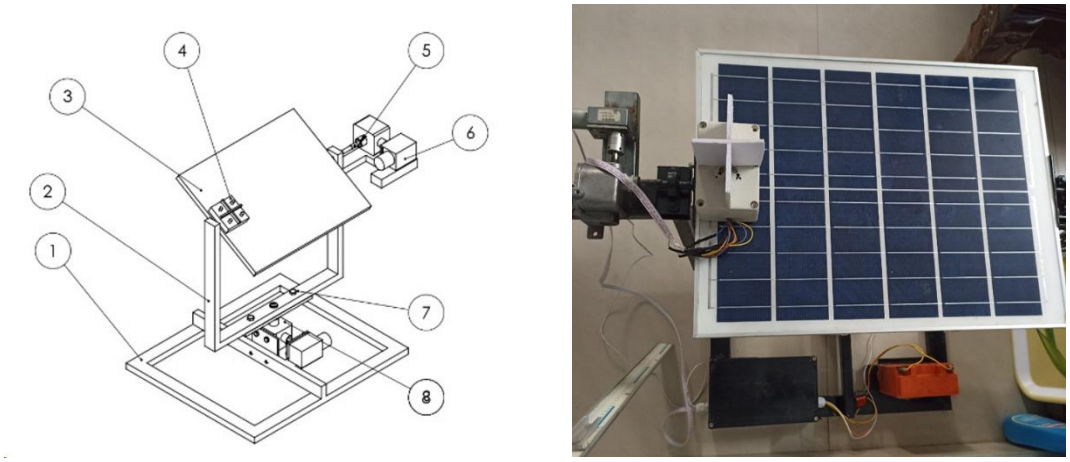

(a) (b)

Figure 6. Prototype: (a) 3D CAD design model; (b) The fully assembled physical prototype.

Table 1. Functional validation results of the dual-axis solar tracking prototype

Test condition	*Sensor response*	*Expected actuator response*	*Observed response*	*Result*
Light source positioned on the left side	*Left LDR values higher than right LDR values*	*JGY370 motor rotates the panel to the left*	*Panel rotated to the left*	*Pass*
Light source positioned on the right side	*Right LDR values higher than left LDR values*	*JGY370 motor rotates the panel to the right*	*Panel rotated to the right*	*Pass*
Light source positioned above the sensor	*Upper LDR values higher than lower LDR values*	*MG996R servo increases the elevation angle*	*Elevation angle increased*	*Pass*
Light source positioned below the sensor	*Lower LDR values higher than upper LDR values*	*MG996R servo decreases the elevation angle*	*Elevation angle decreased*	*Pass*
Light distributed approximately equally among four LDRs	*Differences remain within the predefined tolerance*	*Both actuators stop*	*Both actuators remained idle / stopped*	*Pass*

As presented in Table 1, the prototype responded to changes in the light direction by adjusting the panel along the horizontal and vertical axes. When the differences between the LDR signals remained within the predefined tolerance, both actuators stopped to prevent unnecessary oscillation.

3.3. MATLAB/Simulink Simulation Model

A simulation model was developed in MATLAB/Simulink to compare the power and energy of the fixed and dual-axis configurations. The model has two inputs, the irradiance profile Irradiance_G and the simulation clock t. An embedded MATLAB Function block named P_fixed receives both inputs and computes the instantaneous power of the fixed panel from G(t), the cosine of the incidence angle, and the module rating (Figure 7). The power of the ideal dual-axis tracker, P_dual, is computed in the same way with cos θ = 1. Each power signal is then integrated over time by an integrator block to obtain the accumulated energy E_fixed and E_dual (Figure 8), and the signals are logged in the workspace for comparison.

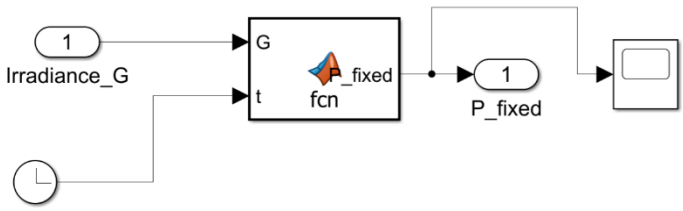

Figure 7. MATLAB/Simulink architecture for the fixed PV configuration evaluation

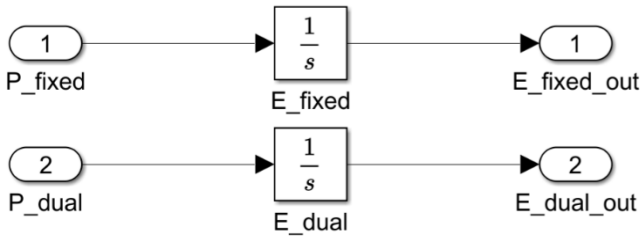

Figure 8. Integration blocks used to compute the accumulated energy of the fixed and ideal dual-axis configurations

The operational power trajectories generated by both the conventional static installation and the active tracking system configurations were synthesized to quantify energy harvest characteristics. The numerical metrics were obtained across the daytime simulation window. The simulated output power of the fixed configuration is shown in Figure 9, while that of the dual-axis tracking configuration is shown in Figure 10. The tracking configuration maintained higher simulated power than the fixed configuration during the morning and afternoon periods, while both configurations approached similar peak values near solar noon. The harvested power profiles validate that during early morning (0h to 3h) and late afternoon (9h to 12h) intervals, the fixed configuration undergoes substantial efficiency degradation due to solar geometric cosine vector deviation. Conversely, the automated tracker continuously optimizes alignment to harvest higher incident irradiance density. To contrast these simulated profiles with international academic validations, the efficiency augmentation aligns with the empirical tracking trends reported by Ponce-Jara et al. [7]. The calculated integration of output profiles indicates that the dual-axis tracker significantly enhances total daily accumulated energy output compared to fixed-angle arrays.

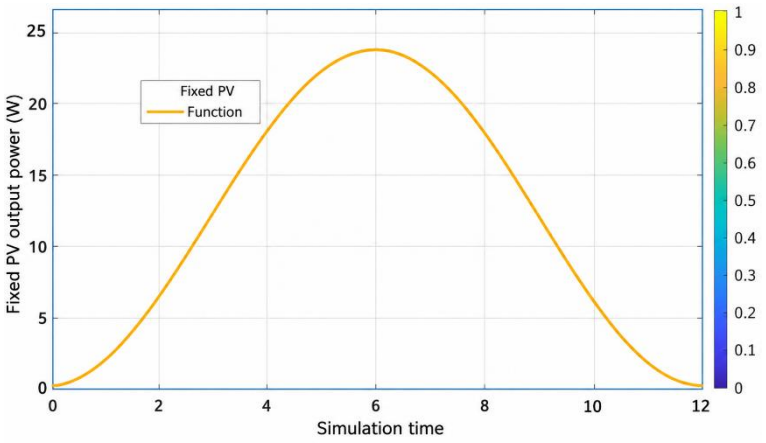

Figure 9. Simulated output power profile of the static fixed photovoltaic configuration

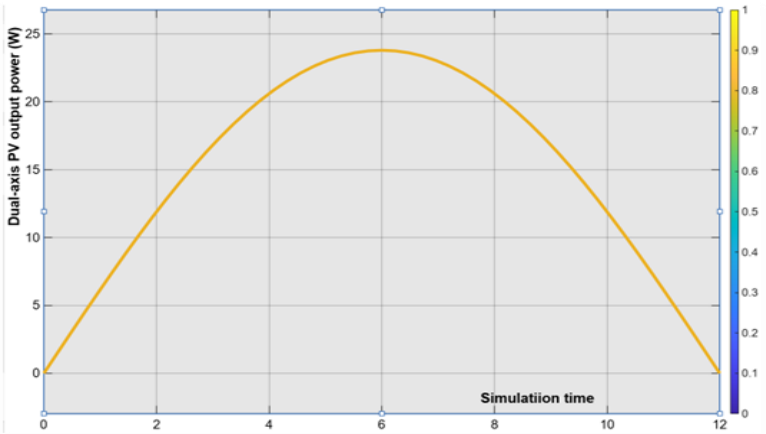

Figure 10. Simulated output power profile of the active dual-axis solar tracking configuration

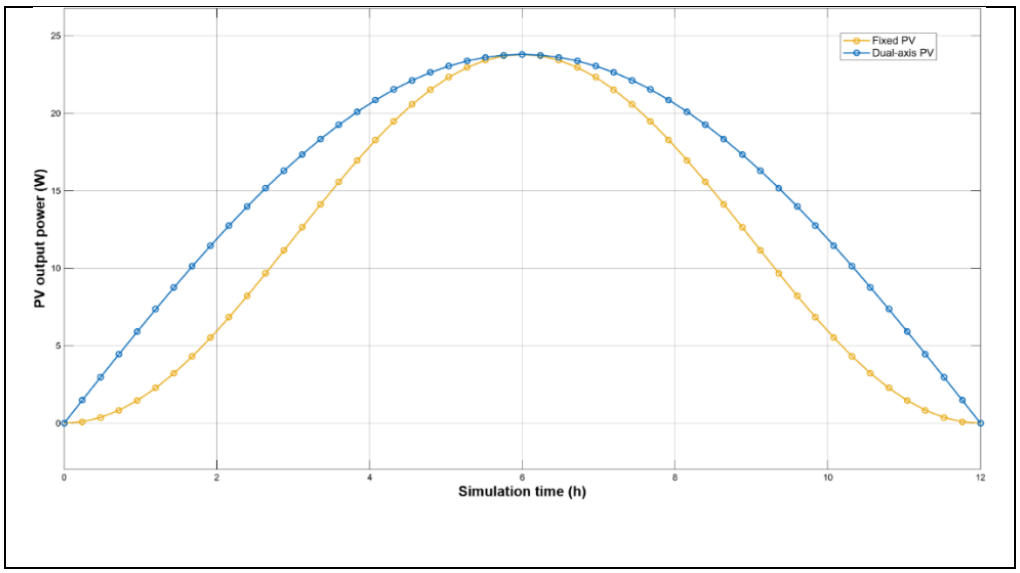

Figure 11. Comparative curves of simulated electrical power profiles between fixed and dual-axis tracking configurations.

Table 2. *Simulated energy generation performance for fixed and dual-axis tracking PV configurations.*

Configuration	Accumulated energy
Fixed PV	*142.80 Wh*
Ideal dual-axis tracking PV	*181.819 Wh*
Absolute increase	*39.019 Wh*
Relative improvement	*27.324%*

The dynamic power generation profile of both the fixed-tilt arrangement and the active dual-axis tracking architecture was evaluated across a continuous twelve-hour simulated daytime window. The resulting curve plots demonstrate a visible power enhancement achieved by the tracking configuration, particularly during the early morning and late afternoon intervals. During these boundary hours, the fixed system suffers severe geometric cosine losses due to the high solar incidence angle, whereas the tracker maintains continuous perpendicular alignment. The alignment allows the 28 W polycrystalline panel to operate near its theoretical maximum capacity for an extended duration, as visualized in the comparative curves of Figure 11.

The simulation results show that the dual-axis tracking photovoltaic system produced higher output power than the fixed photovoltaic system during most daytime periods. The improvement was more evident in the morning and afternoon, when the incidence angle between sunlight and the fixed panel was larger. The accumulated daily energy of the tracking system was then compared with that of the fixed system to determine the percentage energy gain. To quantitatively evaluate the performance enhancement, the accumulated daily energy outputs of both the static fixed panel and the ideal dual-axis tracking system were calculated over the 12-hour simulation period. A detailed comparative summary of these energy yields and the resulting efficiency gain is presented in Table 2.

Over the simulated 12-h daytime period, the accumulated energy increased from 142.800 Wh for the fixed PV configuration to 181.819 Wh for the idealized dual-axis tracking configuration. This represents an absolute increase of 39.019 Wh and a relative improvement of 27.324%.

3.4. Discussions

The results show that the prototype responds correctly to the light direction (Table 1) and that, under ideal tracking, the simulated energy yield is higher than that of a fixed panel (Table 2). The gain comes mainly from the morning and afternoon periods, when the fixed panel has a large incidence angle (Figure 11), so it depends on the fixed-panel tilt and azimuth, the location, and the season used as the baseline. The simulation also links the prototype to an expected energy gain, which is missing in many low-cost Arduino–LDR studies that only confirm actuator movement [2], [9]. Gains reported for dual-axis trackers vary with location, season, and test conditions [4], [5], [7], so the 27.324% obtained here should be read as a case-specific estimate and not as a general value.

The findings should be interpreted within the scope of this study, which has three main boundaries. First, the 27.324% gain is an upper-bound estimate, because the simulation assumes ideal tracking and does not subtract the energy used by the actuators and control electronics. Second, the prototype was validated in the laboratory with an artificial light source, and the simulated results have not yet been compared with outdoor measurements over a full day. Third, the simulation represents one idealized daytime window and does not include cloud cover, to which LDR-based sensing is more sensitive. These boundaries do not change the main outcome, namely that cosine losses explain the gain of the tracker in Figure 11, and they define the next steps: outdoor tests against a fixed reference panel with measured power, inclusion of actuator energy in the net-gain calculation, and evaluation of astronomical or hybrid algorithms to reduce unnecessary actuator movement.

4. Conclusion

This study designed, implemented, and evaluated a low-cost automatic dual-axis solar tracking system for small-scale PV applications. The prototype, based on an Arduino UNO R3, a four-quadrant LDR sensor array, and two-axis electromechanical actuators, responded correctly to the light direction in all five laboratory test conditions using an artificial light source. The MATLAB/Simulink comparison under identical input conditions showed that the ideal dual-axis configuration increased the accumulated energy over a simulated 12-hour daytime period from 142.800 Wh to 181.819 Wh, a relative improvement of 27.324%, mainly through the recovery of cosine losses in the morning and afternoon. Because the simulation assumes ideal tracking and does not include the energy consumed by the actuators and the control electronics, this value is an upper-bound estimate and not a measured field gain. In addition, the prototype has not yet been tested outdoors, and LDR-based sensing may be less robust under variable lighting. Future work will include outdoor measurements against a fixed reference panel, the inclusion of actuator energy in the net-gain calculation, and the evaluation of astronomical or hybrid control algorithms to reduce unnecessary actuator movement.

Acknowledgement

This research was supported and funded by the Faculty of Engineering and Food Technology, and the University of Agriculture and Forestry, Hue University, under the Student Scientific Research Project framework in 2023, grant number DHL2023-CKCN-SV-04. The authors would like to express their deepest gratitude to the institutions for providing the financial support and facilities to complete this research.

CReDiT Author Statement

Bui Hoang Man: Methodology, Investigation, Validation. **Tran Van Duc:** Methodology, Investigation, Validation. **Nguyen Huu Bao Thinh:** Methodology, Investigation, Validation. **Phan Ton Thanh Tam:** Software, Writing – Original Draft. **Nguyen Thi Kim Anh:** Software, Writing – Original Draft. **Ho Van Dung:** Conceptualization, Methodology, Software, Formal Analysis, Supervision, Writing – Original Draft, Writing – Review & Editing. All authors have read and approved the final version of the manuscript.

Declaration of Competing Interest

The authors declare that they have no known competing financial interests or personal relationships that could have appeared to influence the work reported in this paper.

References

[1] Krismadinata, N. A. Rahim, H. W. Ping, and J. Selvaraj, "Photovoltaic Module Modeling using Simulink/Matlab," *Procedia Environmental Sciences*, vol. 17, pp. 537–546, Jan. 2013, doi: 10.1016/J.PROENV.2013.02.069.

[2] C. H. Pardosi, M. Siregar, and L. W. Pandjaitan, "Design and Implementation of A Dual-Axis Solar Tracking System using Arduino Uno Microcontroller," *Jurnal ELTIKOM : Jurnal Teknik Elektro, Teknologi Informasi dan Komputer*, vol. 8, no. 1, pp. 44–56, Jun. 2024, doi: 10.31961/ELTIKOM.V8I1.1105.

[3] M. Nfaoui and K. El-Hami, "Optimal tilt angle and orientation for solar photovoltaic arrays: case of Settat city in Morocco," *International Journal of Ambient Energy*, vol. 41, no. 2, pp. 214–223, Jan. 2020, doi: 10.1080/01430750.2018.1451375.

[4] K. Kumba, P. Upender, P. Buduma, M. Sarkar, S. P. Simon, and V. Gundu, "Solar tracking systems:

Advancements, challenges, and future directions: A review," *Energy Reports*, vol. 12, pp. 3566–3583, Dec. 2024, doi: 10.1016/J.EGYR.2024.09.038.

[5] R. Sadeghi, M. Parenti, S. Memme, M. Fossa, and S. Morchio, "A Review and Comparative Analysis of Solar Tracking Systems," *Energies 2025, Vol. 18, Page 2553*, vol. 18, no. 10, p. 2553, May 2025, doi: 10.3390/EN18102553.

[6] E. K. Mpodi, Z. Tjiparuro, and O. Matsebe, "Review of dual axis solar tracking and development of its functional model," *Procedia Manufacturing*, vol. 35, pp. 580–588, Jan. 2019, doi: 10.1016/J.PROMFG.2019.05.082.

[7] M. A. Ponce-Jara, C. Velásquez-Figueroa, M. Reyes-Mero, and C. Rus-Casas, "Performance Comparison between Fixed and Dual-Axis Sun-Tracking Photovoltaic Panels with an IoT Monitoring System in the Coastal Region of Ecuador," *Sustainability 2022, Vol. 14, Page 1696*, vol. 14, no. 3, p. 1696, Feb. 2022, doi: 10.3390/SU14031696.

[8] A. Priyam, "Solar Tracking Systems – A Review," *Journal of Mines, Metals and Fuels*, vol. 71, no. 10, pp. 1725–1736, Dec. 2023, doi: 10.18311/JMMF/2023/35863.

[9] M. Nur, A. Mohd, A. Jumaat, C. Rimong, A. Jawa, and S. A. Jumaat, "Dual axis solar tracker with IoT monitoring system using arduino," *International Journal of Power Electronics and Drive Systems (IJPEDS)*, vol. 11, no. 1, pp. 451–458, Mar. 2020, doi: 10.11591/IJPEDS.V11.I1.PP451-458.

[10] S. T.-H. Lin, X.-Q. Lin, W.-L. Hsu, C.-M. Hsu, and C.-F. Yang, "Design of a Dual-axis Solar Tracking Mechanism," *Sensors and Materials*, vol. 38, no. 1, pp. 363–373, 2026, doi: 10.18494/SAM5785.

[11] F. Zharfa Athara, F. Athalla Putra, M. Hendra Kurniawan, M. David Praskadana, and A. Arfriandi, "Dual Axis Solar Tracker with Arduino-Based Voltage Monitoring," *Eksergi*, vol. 22, no. 02, pp. 54–59, May 2026, doi: 10.32497/EKSERGI.V22I02.7559.

[12] M. I. Taha, M. A. Kamel, E. Said, and W. Elmayyah, "Comparative performance evaluation of meta-heuristic optimization algorithms for tuning PID gains in dual-axis solar tracking systems," *Proceedings of the Institution of Mechanical Engineers, Part I: Journal of Systems and Control Engineering*, vol. 240, no. 6, pp. 1001–1018, Jul. 2026, doi: 10.1177/09596518261435665.

[13] K. Chenchireddy, G. B. Mulla, V. Jagan, W. Sultana, S. A. Sydu, and E. Giddalur, "Solar tracker using Arduino microcontroller and light dependent resistor," *International Journal of Power Electronics and Drive Systems (IJPEDS)*, vol. 16, no. 1, pp. 70–75, Mar. 2025, doi: 10.11591/IJPEDS.V16.I1.PP70-75.

[14] J. Rishmany, C. Lahoud, J. Harmouche, R. Imad, and N. Saba, "Advancements in Solar Tracking: A Comprehensive Review of Image-Processing Techniques," *Sustainability 2026, Vol. 18, Page 1117*, vol. 18, no. 2, p. 1117, Jan. 2026, doi: 10.3390/SU18021117.

[15] M. Nfaoui *et al.*, "Comprehensive modeling and simulation of photovoltaic system performance by using matlab/simulink: integrating dynamic meteorological parameters for enhanced accuracy," *Journal of Umm Al-Qura University for Applied Sciences*, vol. 11, no. 3, pp. 633–656, Sep. 2025, doi: 10.1007/S43994-024-00175-5/FIGURES/26.

[16] H. Văn Dũng *et al.*, "Thiết kế và chế tạo máy nghiền hạt ngô trên nguyên lý nghiền kiểu búa," *Tạp chí Chuyên đề*, vol. 8, no. 2, pp. 378–386, Dec. 2025, doi: 10.55401/EM99AS46.

[17] H. V. Dũng, K. A. Sơn, V. C. Anh, L. T. K. Anh, T. N. Cường, and N. X. Cường, "Nghiên cứu, thiết kế và chế tạo máy đóng gói sản phẩm dạng bột với năng suất 200 gói/giờ," *Tạp chí Khoa học và Công nghệ*, vol. 7, no. 5, pp. 89–98, Dec. 2024, doi: 10.55401/FQVNVR16.

[18] P. T. T. Tam, T. X. Loc, P. V. Toan, and H. Van Dung, "Application of Mechanical Design Methods in the Development of a Shiitake Mushroom Stem Grinder for Semi-Industrial-Scale Production of Mushroom Floss," doi: 10.5281/ZENODO.21756826.